Title

Yet more evidence that non-aqueous myelin lipids can be directly imaged with ultrashort echo time (UTE) MRI on a clinical 3T scanner: a lyophilized red blood cell membrane lipid study

Authors

Shin, Soo Hyun

Moazamian, Dina

Suprana, Arya

et al.

Publication Date

2024-08-01

DOI

10.1016/j.neuroimage.2024.120666

Peer reviewed

NeuroImage 296 (2024) 120666

Contents lists available at ScienceDirect

NeuroImage

journal homepage: www.elsevier.com/locate/ynimg

Yet more evidence that non-aqueous myelin lipids can be directly imaged with ultrashort echo time (UTE) MRI on a clinical 3T scanner: a lyophilized red blood cell membrane lipid study

Soo Hyun Shin [a], Dina Moazamian [a], Arya Suprana [a,b], Chun Zeng [a], Jiyo S. Athertya [a], Michael Carl [c], Yajun Ma [a], Hyungseok Jang [a], Jiang Du [a,b,d,*]

[a] Department of Radiology, University of California, San Diego, La Jolla, CA, USA
[b] Shu Chien-Gene Lay Department of Bioengineering, University of California, San Diego, La Jolla, CA, USA
[c] GE Healthcare, San Diego, CA, USA
[d] Radiology Service, Veterans Affairs San Diego Healthcare System, La Jolla, CA, USA

ARTICLE INFO

Keywords:
UTE
RBC
Membrane lipid
Myelin, T_2*, T_1

ABSTRACT

Direct imaging of semi-solid lipids, such as myelin, is of great interest as a noninvasive biomarker of neurodegenerative diseases. Yet, the short T_2 relaxation times of semi-solid lipid protons hamper direct detection through conventional magnetic resonance imaging (MRI) pulse sequences. In this study, we examined whether a three-dimensional ultrashort echo time (3D UTE) sequence can directly acquire signals from membrane lipids. Membrane lipids from red blood cells (RBC) were collected from commercially available blood as a general model of the myelin lipid bilayer and subjected to D_2O exchange and freeze-drying for complete water removal. Sufficiently high MR signals were detected with the 3D UTE sequence, which showed an ultrashort T_2* of ~77–271 μs and a short T_1 of ~189 ms for semi-solid RBC membrane lipids. These measurements can guide designing UTE-based sequences for direct in vivo imaging of membrane lipids.

1. Introduction

A significant portion of the molecular composition of cell membranes and myelin consists of the lipid bilayer. The typical cell membrane differs from myelin in the overall lower proportion of lipids and the ratio of three major classes of lipid components. The cell membrane has 25 % cholesterol, 65 % phospholipids, and 10 % glycolipids, while in myelin the ratio is closer to 40 %:50 %:20 %, respectively (Poitelon et al., 2020). Nevertheless, the lipid bilayer is the basic structure of all cell membranes and myelin. Myelin sheath is a modified cell membrane that wraps layer-by-layer around the nerve axon (Kister and Kister, 2022). The membrane lipids may serve as biomarkers of neurological diseases involving apoptosis and demyelination, such as multiple sclerosis (Devarajan, 2005; Lucchinetti et al., 2000). Currently, the integrity of membrane lipids can be probed only by biopsy, an invasive procedure prone to sampling errors. Thus, a noninvasive imaging method that can selectively monitor membrane lipids will be a valuable diagnostic tool for many neurological degenerative diseases.

Magnetic resonance imaging (MRI) has been widely studied for acquiring anatomical and morphological information and quantitating molecular composition and microstructural integrity via diverse contrast mechanisms. For monitoring membrane lipids and myelination levels in the brain, several MRI approaches have been suggested, such as magnetization transfer (MT) imaging, bound water (e.g., myelin water) imaging, and chemical exchange saturation transfer (CEST) imaging (Swanson et al., 2017; Lee et al., 2021; Zhao et al., 2023). Although these methods have demonstrated the potential of quantitatively measuring the membrane lipids and myelin, they are fundamentally indirect measurements that depend on the exchange between free water protons and membrane protons or on probing surrogate bound water pools associated with membrane lipids. This dependency on the exchange between two proton pools and surrogate markers complicates the quantification of membrane lipid and myelin content. Furthermore, it is difficult to evaluate the quality of membrane lipids and myelin, such as their T_1 and T_2* relaxation times.

For direct imaging of membrane lipids, which possess very short T_2 relaxation times, ultrashort echo time (UTE) MRI pulse sequences can be used (Waldman et al., 2003; Horch et al., 2011; J. Du et al., 2014; Y.-J.

* Correspondence to.
E-mail address: jiangdu@health.ucsd.edu (J. Du).

https://doi.org/10.1016/j.neuroimage.2024.120666
Received 21 August 2023; Received in revised form 16 May 2024; Accepted 31 May 2024
Available online 1 June 2024

Ma et al., 2020; Ma et al., 2022; Wilhelm et al., 2012). UTE MRI has been demonstrated as a useful platform for imaging short T_2 tissues such as bone, tendon, and myelin, as well as for characterizing their relaxation properties (Y.-J. Ma et al., 2020; Afsahi et al., 2022; J. Du et al., 2014; Y. Ma et al., 2020; Chu and Williams, 2019; Du et al., 2010). Myelin has been of great interest as a target for this technique to measure relaxation times in an effort to develop UTE imaging as a sensitive diagnostic tool for neurodegenerative diseases such as multiple sclerosis (van der Weijden et al., 2021). Various dehydrated ex vivo myelin samples were extensively studied to measure their T_1 and T_2* relaxation times via these sequences. However, the measurements highly depend on the sample preparation and image acquisition/analysis methods (J. Du et al., 2014; Wilhelm et al., 2012; MacKay et al., 2006; E.L. Baadsvik et al., 2023). Myelin samples may also lose their unique multilamellar membrane structure during the preparation, which can significantly alter the MR relaxation properties (Shatil et al., 2018). Thus, to develop UTE as a robust and selective imaging method for myelin, the relaxation times should be measured with a more generalized form of membrane lipids that maintains the original structure during the sample preparation.

Here, we demonstrate the feasibility of directly imaging membrane lipids via the UTE sequence using red blood cell (RBC) membranes and measuring their relaxation properties. RBC membranes have been widely studied for preparing ghost membranes that preserve their original form (Schwoch and Passow, 1973; Deák et al., 2015). The prepared samples were completely dehydrated to ensure the measured MR signals were only from non-aqueous protons in the RBC membrane samples. T_1 and T_2* relaxation times were measured using different analysis methods and compared with previous studies on myelin samples.

2. Materials and methods

2.1. RBC membrane preparation

The RBC membranes were collected from commercially available blood (Lampire Biological Laboratories, Pipersville, PA). The plasma and buffy coat were removed by centrifugation, and the remaining RBCs were washed with Tris buffer (0.176 M, pH 7.6). Cell membranes were collected by mixing with Tris buffer (11.35 mM, pH 7.6) for 5 min at 4 °C and centrifuging at 20,000 g for 30 min. The collected RBC lipid membrane was suspended in D_2O for 24 h, centrifuged, and freeze-dried overnight in a 1 mL syringe. The D_2O suspension and freeze-drying were repeated twice to remove water completely, followed by air removal via compressing and capping.

2.2. MR image acquisition and analysis

The RBC membrane sample in the 1 mL syringe (length: 10.2 cm, inner diameter: 4.78 mm) was placed parallel to the scanner bore in a wrist coil and scanned at 3T (GE Healthcare Technologies Inc, Milwaukee, WI) at room temperature. Images were acquired using a 3D UTE sequence with TR = 30 ms, TE = 32 μs, acquisition matrix size = 64 × 64 × 20, field of view (FOV) = 80 mm, slice thickness = 10 mm, number of averages = 1, and sampling bandwidth = 125 kHz. The sequence was repeated with seven different echo times (TE = 32, 64, 150, 200, 400, 600, and 800 μs) to measure the T_2* of the RBC membrane lipid. T_2* was measured via both exponential (mono and bicomponent) and bi-component (e.g., long T_2* and short T_2* components) super-Lorentzian fitting of images acquired with 7 different TEs. Normalized root mean squared error (NRMSE) was used to evaluate the goodness-of-fit.

A variable flip angle (VFA) approach with the same UTE readout was used to measure the T_1 of the RBC membrane lipid, using nominal flip angles of 1°, 5°, 10°, 15°, 20°, and 25° TR and TE were fixed to 30 ms and 32 μs, respectively. Nominal flip angles used for T_1 measurement were corrected by considering T_2* decay during radiofrequency (RF) pulse excitation (Carl et al., 2010). T_2* measured from bi-exponential fitting was applied for this purpose, as the T_2* decay model is based on the assumption of exponential decay.

2.3. Exponential fitting for T_2* measurement

T_2* relaxation time was first measured via conventional exponential fitting. A custom-written MATLAB (MathWorks, Natick, MA) code was used for the fitting. The same UTE dataset with 7 different TEs was fit twice using a mono-exponential model and then a bi-exponential model (long and short T_2* compartments). Bi-exponential fitting was performed to examine whether residual free water remained in the sample. The trust-region algorithm was used for the fitting process, with the boundary for short T_2* ranging from 0.1 μs to 10 ms.

2.4. Super-Lorentzian fitting for T_2* measurement

As ultrashort T_2* species such as myelin are known to have super-Lorentzian line shape, we also fitted the same UTE dataset with 7 different TEs into the super-Lorentzian model as previously described using a MATLAB code (Wilhelm et al., 2012; Weiger et al., 2020). Similar to bi-exponential fitting, super-Lorentzian fitting was also performed in a two-component model, with one component representing a residual free water pool with an exponential line shape. Similar to bi-exponential fitting, a trust-region algorithm was used for the fitting with the boundaries for T_2* of super-Lorentzian pool ranging from 1 μs to 1 ms.

2.5. Data and code availability statement

The supporting data, the reported findings, and the code used to analyze the data are available from the corresponding author upon request.

3. Results

The membrane lipid signal was well detected with the 3D UTE sequence (Fig. 1A). The T_2* of the membrane lipid was measured to be 271 ± 8 μs based on mono-exponential fitting (Fig. 1B), and 252 ± 51 μs via bi-exponential fitting with the relative amplitude of short T_2* component being approximately 97 % (NRMSE = 0.0162; Fig. 1B). The T_2* from the super-Lorentzian fitting was measured to be 77±5 μs, with the amplitude of the short T_2* component being 95 % (NRMSE = 0.0348; Fig. 1C).

The raw images for the T_1 measurement showed decreasing signal intensities with flip angles (Fig. 2A). Without flip angle correction, the T_1 was measured to be 127 ± 7 ms. Correcting flip angles using T_2* measurement from bi-exponential fitting (T_2* = 252 ± 51 μs) updated the T_1 value to 189 ± 7 ms (Fig. 2B).

Table 1 summarizes the measured T_2* values of the RBC membrane lipids in this study and the T_2* values of non-aqueous myelin lipid protons reported in the literature. The T_2* values measured with the exponential and super-Lorentzian fitting are largely consistent with values reported in previous studies. The exponential model provides consistently longer T_2* values than the super-Lorentzian model.

4. Discussion

In this study, we demonstrated the direct detection of membrane lipids and measurements of their MR relaxation times via UTE MRI on a clinical whole-body scanner. The detection of MR signals from completely dehydrated RBC membrane lipids parallels the previous UTE studies on bovine myelin lipid imaging (Horch et al., 2011; Wilhelm et al., 2012; Sheth et al., 2016). The ultrashort T_2* of ~77–271 μs and short T_1 of ~189 ms for semi-solid RBC membrane lipids are also similar

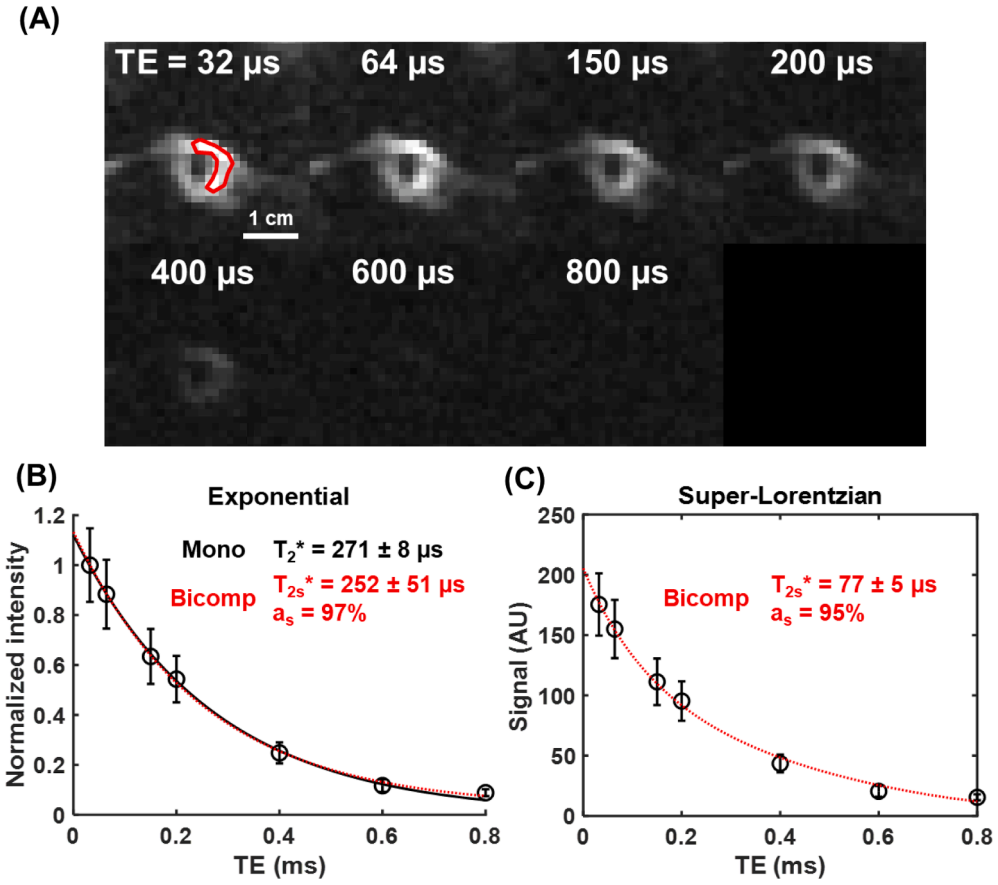

Fig. 1. Direct UTE imaging of red blood cell (RBC) membrane lipids and T_2* measurements. (A) Raw images of the RBC membrane lipid sample at different echo times. A red region-of-interest (ROI) was used to measure T_2* relaxation times via exponential fitting. (B) and bicomponent super-Lorentzian fitting (C). (T_{2s}* = T_2* of short T_2* component. a_s = relative amplitude of short T_2* component).

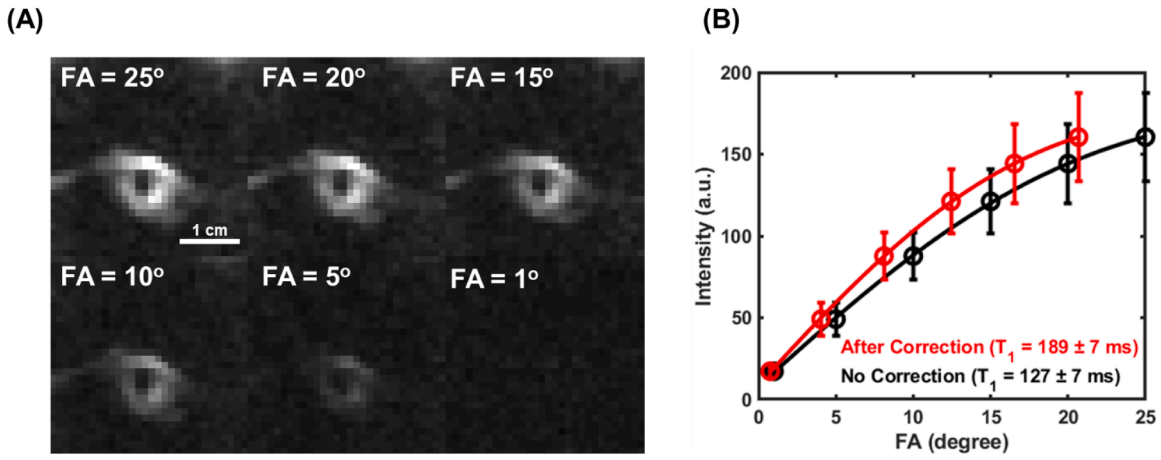

Fig. 2. T_1 measurement of semi-solid RBC membrane protons via variable flip angle (VFA) method. (A) Raw images of RBC membranes over a range of flip angles were used for the T_1 measurement. (B) Comparison of T_1 measurement before and after correction for the T_2* decay during RF excitation. The flip angle correction updates the T_1 measurement from 127 ± 7 ms to 189 ± 7 ms.

to the relaxation times for myelin lipids. Combining D_2O-exchange with freeze-drying of RBC membrane lipid samples guarantees that the MR signals are only generated from semi-solid lipid protons. These results demonstrate that UTE MRI can image non-aqueous RBC membrane lipid protons directly. The relaxation measurements can guide the designing of UTE-based sequences for direct in vivo imaging of membrane lipids.

On top of demonstrating the feasibility of direct detection of semi-solid membrane lipid protons, we also measured the T_1 and T_2* relaxation times of these protons via UTE MRI. The measurement of these relaxation times is crucial for optimizing the UTE sequence to achieve the highest possible signal-to-noise ratio (SNR) and contrast-to-noise ratio (CNR) (Young et al., 2020). Considering the very short T_2 relaxation times of semi-solid protons, it is of critical importance to consider the following factors in the morphological and quantitative imaging of

Table 1
Comparison of T_2* relaxation time of red blood cell (RBC) membrane lipids measured in this study with previous studies on myelin lipids, ex vivo brain samples, and in vivo brain scans

Study	Sample preparation	Acquisition and analysis method	Value
Horch et al., 2011	Myelin extract	200 MHz NMR CPMG and FID Exponential and Gaussian	50–1000 μs
Sheth et al., 2016	Bovine myelin lipid (powder or in D_2O)	2D UTE at 3T Exponential	130–300 μs
Weiger et al., 2020	Porcine brain sample	3D ZTE at 3T Lorentzian and super-Lorentzian	7.5–101 μs
Fan et al., 2017	Ovine brain sample	IR-UTE	200–300 μs
Wilhelm et al., 2012	Bovine myelin extract	2D and 3D UTE at 9.4T Super-Lorentzian	8–1000 μs
Ma et al., 2020	Rat spinal cord In vivo human brain scan	STAIR-UTE at 3T Exponential	~220 μs
Seifert et al., 2017	Ovine spinal cord myelin extract in D_2O	9.4T NMR Super-Lorentzian	5–30 μs
This study	**RBC membrane**	**3D UTE at 3T Exponential and Super-Lorentzian**	**77–271 μs**

CPMG = Carr-Purcell-Meiboom-Gill sequence. FID = free-induction decay. UTE = ultrashort echo time. ZTE = zero echo time. IR-UTE = inversion recovery-UTE, STAIR-UTE = short TR adiabatic inversion recovery-UTE.

membrane lipids. First, the echo time should be kept as short as possible to minimize short T_2 signal decay. Conventional spin echo and gradient echo sequences with TEs of several milliseconds or longer cannot detect much signal from semi-solid membrane lipid protons. Second, the data sampling window should be kept relatively short to minimize signal loss during spatial encoding (Rahmer et al., 2006). Radial ramp sampling used in UTE imaging typically suffers from more spatial blurring in imaging short T_2 tissues than zero echo time (ZTE) type sequences (E.L. Baadsvik et al., 2023; Weiger et al., 2020; Rahmer et al., 2006; Seifert et al., 2017). Third, the radiofrequency (RF) pulse should be kept short to minimize transverse relaxation during excitation (Carl et al., 2010). A high B_1 field is preferred for more accurate excitation of membrane lipids. A short rectangular pulse with the highest B_1 available on a clinical MR system is typically employed for direct imaging of myelin and membrane lipids (Wilhelm et al., 2012). Fourth, efficient water signal suppression is required for high contrast imaging of myelin and membrane lipids, as the water signal is far higher than that of myelin and membrane lipids (Fan et al., 2018).

The measured T_1 and T_2* relaxation times can also be utilized to implement this UTE sequence for in vivo imaging of membrane lipids (Young et al., 2020). UTE imaging of short T_2 tissues in vivo often involves magnetization preparations such as inversion recovery or the post-processing of acquired images such as echo image subtractions to acquire positive contrast from the target short T_2 tissues (Jang et al., 2020; Ma et al., 2021). For the effective suppression of signals from long T_2 tissues, the adiabatic inversion recovery preparation followed by echo subtraction seems more efficient than other approaches, such as long T_2 signal saturation (Larson et al., 2006), or subtraction of longer echo images from short echo images (Weiger et al., 2020), largely because of the insensitivity of adiabatic inversion pulses to B_1 and B_0 inhomogeneities (Garwood and DelaBarre, 2001), thereby providing uniform inversion and nulling of water signals. However, the inversion recovery time and echo spacings should be carefully chosen based on the T_1 and T_2* relaxation times of the tissues (Y.-J. Ma et al., 2020). The T_1 and T_2* relaxation times of the RBC membrane from this study can serve as a good starting point for future studies on selective in vivo imaging of membrane lipids (Young et al., 2020). Still, it should be noted that the differences in membrane lipid compositions and microenvironment between different tissues (e.g., RBC membrane vs. myelin) can lead to different T_1 and T_2* relaxation times, requiring fine measurements for each tissue type of interest. The magnetization exchange between different components can further complicate the measurement (especially T_1 relaxation time) and analysis of relaxation properties, as these components can be excited unequally by an RF pulse (Soustelle et al., 2023). We also measured the relaxation properties at room temperature. For in vivo imaging, it is reasonable to extrapolate that the T_1 will be longer than our measurements due to the higher temperature. The oxygen saturation level can be a confounding factor in vivo, as the reduction of T_2* in the presence of deoxyhemoglobin is well known as the basis of the blood oxygen level-dependent (BOLD) effect. The iron in hemoglobin may also further shorten the T_2* relaxation time. However, the blood still has a relatively long T_2/T_2* so that the signals from blood can be suppressed by using an adiabatic inversion pulse and an appropriate nulling time point, enabling selective UTE imaging of ultrashort T_2* signals from RBC membranes (Ma et al., 2021; Y.-J. Ma et al., 2020).

We measured T_1 and T_2* of RBC membrane lipids, which were around 189 ms and 77–271 μs, respectively. These measurements align with previous reports on the T_1 and T_2* relaxation times of ex vivo myelin powder samples or brain white matter (Horch et al., 2011; Wilhelm et al., 2012; J. Du et al., 2014; MacKay et al., 2006; Weiger et al., 2020; Sheth et al., 2016; He et al., 2017; Sheth et al., 2017; Fan et al., 2017). This alignment of measurements was expected as both myelin sheath and RBC membranes share a similar structure of lipid bilayers. The discrepancy between T_2* measurements from bi-exponential (252 μs) and bicomponent super-Lorentzian (77 μs) fitting was expected, as lipid bilayers show super-Lorentzian line shape and exponential fitting can overestimate the T_2* values (Wennerström, 1973). Despite this difference in T_2* measurements, both models show a similar high amplitude of short T_2* components (97 % from bi-exponential and 95 % super-Lorentzian), cross-validating that the free water was almost completely removed via D_2O exchange and freeze-drying. The T_2* of 77 ± 5 μs from super-Lorentzian fitting falls within the range of previously reported myelin T_2*/T_2 values summarized in Table 1 (e.g., ~50 μs (MacKay et al., 2006), 7.5–101 μs (Weiger et al., 2020), 50–1000 μs (Horch et al., 2011), 150–250 μs (J. Du et al., 2014; Sheth et al., 2016; Y.-J. Ma et al., 2020; He et al., 2017; Sheth et al., 2017; Fan et al., 2017), or 8 μs-26 ms with ~90 % of the myelin T_2* < 1000 μs (Wilhelm et al., 2012)). Yet, other studies used three-component super-Lorentzian fitting and revealed the existence of a very short T_2* (~5 μs) component, which is unlikely to be detected by our UTE sequence with TE of 32 μs at a whole body scanner (E.L. Baadsvik et al., 2023; E.L. Baadsvik et al., 2023). This wide range of T_2* values indicates the existence of multiple components in myelin and complicates the procedure of assigning the molecular origin of each T_2* component. Similarly, RBC membrane components other than lipids, such as actin filaments, may also contribute to the UTE signals detected in this study, analogous to the fact that myelin basic proteins can also contribute to UTE signals of myelin. Different fitting approaches (mono vs. bi-component, exponential vs. super-Lorentzian) employed in this study may be useful for probing different components in RBC membranes and myelin based on their molecular mobility and T_2* relaxation. Considering that we used completely dehydrated RBC membranes, the solid-state NMR spectrum can help resolve the ambiguity of line shape, identify different components, and measure their T_2* relaxation.

Meanwhile, a recent study by Seifert et al. demonstrated an excellent mono-exponential fit to the first 2 ms of 3T free induction decay (FID) data, yielding a T_2* of 238 ms and R^2 of 0.994[31]. In contrast, the super-Lorentzian fit produced an R^2 value of 0.9992. The super-Lorentzian model only slightly increased the R^2 value (0.9992 vs. 0.994, or 0.5 % increase) over the mono-exponential fit at 3T. In other words, the much-simplified mono-exponential model works very well in quantifying myelin T_2* at 3T. It is likely that the super-Lorentzian model might be more accurate in fitting the supershort T_2* (~10 μs) components, while the mono-exponential model might work well for the ultrashort T_2* (~100–200 μs) components, as suggested by the equally well fitted

super-Lorentzian model and mono-exponential model in the Seifert study and our current study. The strong spatial blurring might be a key factor explaining the similar good fitting using both models. The sampling window is on the order of hundreds of microseconds in typical UTE or ZTE imaging, which is much longer than the supershort T_2* components and significantly longer than the ultrashort components, leading to strong spatial blurring. A numerical simulation study might help explain this phenomenon, especially on whether the ~10 μs components could be spatially encoded and potential errors in T_2* and T_1 quantification.

For the T_1 measurement, we used the VFA method with flip angle correction regarding the rapid T_2* decay during the RF excitation. The elongated T_1 relaxation time after the correction indicates the need for the flip angle correction to measure T_1 relaxation time in the case of short T_2 tissues. The updated T_1 value of 189 ms roughly aligns with the previously reported T_1 relaxation times of 150–230 ms from the four-pool model analysis of white matter samples from a fresh bovine brain (Manning et al., 2021), and 197–248 ms from single exponential recovery fitting of long-T_2 suppressed UTE images of white matter in healthy volunteers (J. Du et al., 2014). To enhance the precision of VFA-based T_1 measurement, acquiring a reference amplitude and including higher flip angles can be helpful as we did not observe the peak amplitude in the VFA curve shown in Fig. 2. Other image acquisition and analysis methods can also be tested for cross-validation, such as the variable repetition time (VTR) method and multi-pool analysis (Ma et al., 2018; Reynolds et al., 2023).

We used the RBC membrane as a general model of membrane lipids in tissue. The protocol of preparing "ghost membranes" from RBCs using hypertonic solution has been well established over decades and is widely utilized in camouflaged nanoparticle synthesis these days (Schwoch and Passow, 1973; Luk and Zhang, 2015; Xia et al., 2019). This protocol is well suited for our study as the original structure of lipid bilayers of RBC membranes is relatively well preserved. The relaxation properties of myelin powder have been extensively studied in light of applications in neurodegenerative diseases such as multiple sclerosis. However, whether the unique multilamellar lipid bilayer structure of myelin is preserved in a powder form is uncertain, questioning whether the measurements from ex vivo samples are comparable to the true relaxation properties of semi-solid myelin protons in vivo. Although further studies are needed, the measurements from RBC membranes match well with previous reports on ex vivo myelin samples, implying that the loss of structural integrity of myelin did not heavily affect the previous T_1 and T_2* measurements.

These relaxation measurements from RBC membrane samples can be used to optimize the UTE sequence for direct in vivo imaging of membrane lipids and myelin in general, owing to their structural and compositional similarities. Current MRI methods for detecting demyelination are either non-specific to myelin or indirect, probing general T_2 or T_2* changes. Similar to approaches discussed above for general membrane lipid imaging, the same principles can be applied for direct imaging of myelin—suppressing long T_2 components utilizing the relaxation times measured in this study and directly detecting signals from myelin protons with UTE readout. UTE sequences have distinct advantages over conventional MRI sequences, which are indirect and have difficulty quantifying membrane lipid content, especially regarding T_1 and T_2* relaxation times. This approach of directly imaging myelination may not only improve the diagnosis of neurodegenerative diseases but also facilitate the development of novel therapies for such diseases by offering reliable noninvasive methods of assessing therapeutic efficacy and safety profile.

In future studies, the accuracy of T_2* measurement should be improved by acquiring more TEs. In this study, we only used 7 TEs for the T_2* measurement. This T_2* measurement will also affect the T_1 measurement through the VFA approach, as the flip angle should be corrected due to fast transverse relaxation during the RF excitation for ultrashort T_2 tissues. The T_1 was updated to 189 ± 7 ms from 127 ± 7 ms after the flip angle correction based on the T_2* measurement via bi-exponential fitting. A signal decay model that accounts for super-Lorentzian line shape may allow more accurate flip angle correction and subsequent T_1 measurement. On top of acquiring more TEs, the chemical shift of membrane lipids should also be considered for more accurate T_2* measurement. Each of the different chemical compositions and functional groups in the lipid membrane can be modeled as a separate super-Lorentzian function with different resonant frequencies. In this study, only one super-Lorentzian function was used for the fitting, and the relative chemical shift from the long T_2 component (modeled as an exponential function) was not considered for T_2* fitting. Taking the chemical shift into account may reveal super-Lorentzian components with even shorter T_2* relaxation times (Seifert et al., 2017). Furthermore, a Gaussian lineshape might be more appropriate for the supershort T_2* (~5 μs) components. A systematic study should be performed to compare the Lorentzian, super-Lorentzian, and Gaussian lineshapes for different T_2* components of the non-aqueous cell membrane and myelin lipid protons.

Lastly, the correction of UTE-associated spatial blurring (e.g., T_2* and point-spread function (PSF) blurring) may lead to a higher accuracy in relaxation time measurements. PSF blurring is a well-known challenge in UTE MRI. In this study, no PSF correction was applied. All the UTE images with different flip angles and echo times were subject to similar PSF blurring. Future studies are needed to correct PSF blurring and assess its effect on relaxation time measurements. T_2* blurring can be minimized via several methods, including high amplitude gradients, correction of phase and T_2* along the readout, and T_2-adapted sampling (Rahmer et al., 2006).

5. Conclusion

We demonstrated the feasibility of 3D UTE sequences to directly image the semi-solid membrane lipids. We also measured the T_1 (~189 ms) and T_2* (77–271 μs) of the RBC membrane lipids that could be utilized to optimize UTE sequences for in vivo membrane lipid imaging.

CRediT authorship contribution statement

Soo Hyun Shin: Writing – review & editing, Writing – original draft, Validation, Methodology, Investigation, Formal analysis, Data curation, Conceptualization. **Dina Moazamian:** Validation, Methodology, Data curation. **Arya Suprana:** Validation, Methodology, Investigation. **Chun Zeng:** Investigation, Data curation. **Jiyo S. Athertya:** Investigation, Funding acquisition, Formal analysis, Data curation. **Michael Carl:** Supervision, Software, Methodology. **Yajun Ma:** Writing – review & editing, Supervision, Software, Resources, Methodology. **Hyungseok Jang:** Writing – review & editing, Supervision, Software, Investigation. **Jiang Du:** Writing – review & editing, Supervision, Resources, Methodology, Funding acquisition, Conceptualization.

Declaration of competing interest

M.C. is an employee of GE Healthcare. There are no other conflicts of interest to declare.

Data availability

Data will be made available on request.

Acknowledgments

The authors acknowledge grant support from the National Institutes of Health (RF1AG075717 and F32AG082458), VA Clinical Science and Rehabilitation Research and Development Services (Merit Awards I01CX002211), and GE Healthcare.

References

Poitelon, Y., Kopec, A.M., Belin, S., 2020. Myelin fat facts: an overview of lipids and fatty acid metabolism. Cells 9, 812.

Kister, A., Kister, I., 2022. Overview of myelin, major myelin lipids, and myelin-associated proteins. Front. Chem. 10, 1–9.

Devarajan, P., 2005. Cellular and molecular derangements in acute tubular necrosis. Curr. Opin. Pediatr. 17, 193–199.

Lucchinetti, C., et al., 2000. Heterogeneity of multiple sclerosis lesions: implications for the pathogenesis of demyelination. Ann. Neurol. Off. J. Am. Neurol. Assoc. Child Neurol. Soc. 47, 707–717.

Swanson, S.D., et al., 2017. Molecular, dynamic, and structural origin of inhomogeneous magnetization transfer in lipid membranes. Magn. Reson. Med. 77, 1318–1328.

Lee, J., et al., 2021. So you want to image myelin using MRI: an overview and practical guide for myelin water imaging. J. Magn. Reson. Imaging 53, 360–373.

Zhao, Y., Sun, C., Zu, Z., 2023. Assignment of molecular origins of NOE signal at− 3.5 ppm in the brain. Magn. Reson. Med. 90, 673–685.

Waldman, A., et al., 2003. MRI of the brain with ultra-short echo-time pulse sequences. Neuroradiology 45, 887–892.

Horch, R.A., Gore, J.C., Does, M.D., 2011. Origins of the ultrashort-T2 1H NMR signals in myelinated nerve: a direct measure of myelin content? Magn. Reson. Med. 66, 24–31.

Du, J., et al., 2014a. Ultrashort echo time (UTE) magnetic resonance imaging of the short T2 components in white matter of the brain using a clinical 3T scanner. Neuroimage 87, 32–41.

Ma, Y.-J., et al., 2020a. Ultrashort echo time (UTE) magnetic resonance imaging of myelin: technical developments and challenges. *Quant.* Imaging Med. Surg. 10, 1186.

Ma, Y., et al., 2022. Making the invisible visible—Ultrashort echo time magnetic resonance imaging: technical developments and applications. Appl. Phys. Rev. 9.

Wilhelm, M.J., et al., 2012. Direct magnetic resonance detection of myelin and prospects for quantitative imaging of myelin density. Proc. Natl. Acad. Sci. 109, 9605–9610.

Ma, Y.-J., et al., 2020b. Quantitative ultrashort echo time (UTE) magnetic resonance imaging of bone: an update. Front. Endocrinol. (Lausanne). 11, 567417.

Afsahi, A.M., et al., 2022. Ultrashort echo time magnetic resonance imaging techniques: met and unmet needs in musculoskeletal imaging. J. Magn. Reson. Imaging 55, 1597–1612.

Du, J., et al., 2014b. Measurement of T1 of the ultrashort T2* components in white matter of the brain at 3T. PLoS ONE 9, e103296.

Ma, Y., et al., 2020c. Trabecular bone imaging using a 3D adiabatic inversion recovery prepared ultrashort TE Cones sequence at 3T. Magn. Reson. Med. 83, 1640–1651.

Chu, C.R., Williams, A.A., 2019. Quantitative MRI UTE-T2* and T2* show progressive and continued graft maturation over 2 years in human patients after anterior cruciate ligament reconstruction. Orthop. J. Sport. Med. 7, 2325967119863056.

Du, J., et al., 2010. Qualitative and quantitative ultrashort echo time (UTE) imaging of cortical bone. J. Magn. Reson. 207, 304–311.

van der Weijden, C.W.J., et al., 2021. Myelin quantification with MRI: a systematic review of accuracy and reproducibility. Neuroimage 226, 117561.

MacKay, A., et al., 2006. Insights into brain microstructure from the T2 distribution. Magn. Reson. Imaging 24, 515–525.

Baadsvik, E.L., et al., 2023a. Mapping the myelin bilayer with short-T2 MRI: methods validation and reference data for healthy human brain. Magn. Reson. Med. 89, 665–677.

Shatil, A.S., Uddin, M.N., Matsuda, K.M., Figley, C.R., 2018. Quantitative ex vivo MRI changes due to progressive formalin fixation in whole human brain specimens: longitudinal characterization of diffusion, relaxometry, and myelin water fraction measurements at 3T. Front. Med. 5, 31.

Schwoch, G., Passow, H, 1973. Preparation and properties of human erythrocyte ghosts. Mol. Cell. Biochem. 2, 197–218.

Deák, R., et al., 2015. Physicochemical characterization of artificial nanoerythrosomes derived from erythrocyte ghost membranes. Colloids Surf. B Biointerfaces 135, 225–234.

Carl, M., Bydder, M., Du, J., Takahashi, A., Han, E., 2010. Optimization of RF excitation to maximize signal and T2 contrast of tissues with rapid transverse relaxation. Magn. Reson. Med. 64, 481–490.

Weiger, M., et al., 2020. Advances in MRI of the myelin bilayer. Neuroimage 217, 116888.

Sheth, V., et al., 2016. Magnetic resonance imaging of myelin using ultrashort Echo time (UTE) pulse sequences: phantom, specimen, volunteer and multiple sclerosis patient studies. Neuroimage 136, 37–44.

Young, I.R., Szeverenyi, N.M., Du, J., Bydder, G.M., 2020. Pulse sequences as tissue property filters (TP-filters): a way of understanding the signal, contrast and weighting of magnetic resonance images. Quant. Imaging Med. Surg. 10, 1080.

Rahmer, J., Börnert, P., Groen, J., Bos, C., 2006. Three-dimensional radial ultrashort echo-time imaging with T2 adapted sampling. Magn. Reson. Med. An Off. J. Int. Soc. Magn. Reson. Med. 55, 1075–1082.

Seifert, A.C., Li, C., Wilhelm, M.J., Wehrli, S.L., Wehrli, F.W., 2017. Towards quantification of myelin by solid-state MRI of the lipid matrix protons. Neuroimage 163, 358–367.

Fan, S., et al., 2018. Yet more evidence that myelin protons can be directly imaged with Ute sequences on a clinical 3 T scanner: bicomponent analysis of native and deuterated ovine brain specimens. Magn. Reson. Med. 80, 538–547.

Jang, H., et al., 2020. Improved volumetric myelin imaging in human brain using 3D dual echo inversion recovery-prepared UTE with complex echo subtraction. Magn. Reson. Med. 83, 1168–1177.

Ma, Y.-J., et al., 2021. Brain ultrashort T2 component imaging using a short TR adiabatic inversion recovery prepared dual-echo ultrashort TE sequence with complex echo subtraction (STAIR-dUTE-ES). J. Magn. Reson. 323, 106898.

Larson, P.E.Z., et al., 2006. Designing long-T2 suppression pulses for ultrashort echo time imaging. Magn. Reson. Med. An Off. J. Int. Soc. Magn. Reson. Med. 56, 94–103.

Garwood, M., DelaBarre, L., 2001. The return of the frequency sweep: designing adiabatic pulses for contemporary NMR. J. Magn. Reson. 153, 155–177.

Soustelle, L., et al., 2023. Quantitative magnetization transfer MRI unbiased by on-resonance saturation and dipolar order contributions. Magn. Reson. Med. 90, 875–893.

Ma, Y.-J., et al., 2020d. Myelin imaging in human brain using a short repetition time adiabatic inversion recovery prepared ultrashort echo time (STAIR-UTE) MRI sequence in multiple sclerosis. Radiology 297, 392–404.

He, Q., et al., 2017. Direct magnitude and phase imaging of myelin using ultrashort echo time (UTE) pulse sequences: a feasibility study. Magn. Reson. Imaging 39, 194–199.

Sheth, V.R., et al., 2017. Inversion recovery ultrashort echo time magnetic resonance imaging: a method for simultaneous direct detection of myelin and high signal demonstration of iron deposition in the brain–A feasibility study. Magn. Reson. Imaging 38, 87–94.

Fan, S., Ma, Y., Chang, E.Y., Bydder, G.M., Du, J., 2017. Inversion recovery ultrashort echo time imaging of ultrashort T2 tissue components in ovine brain at 3 T: a sequential D2O exchange study. NMR Biomed 30, e3767.

Wennerström, H., 1973. Proton nuclear magnetic resonance lineshapes in lamellar liquid crystals. Chem. Phys. Lett. 18, 41–44.

Baadsvik, E.L., et al., 2023b. Quantitative magnetic resonance mapping of the myelin bilayer reflects pathology in multiple sclerosis brain tissue. Sci. Adv. 9 (32), eadi0611.

Manning, A.P., MacKay, A.L., Michal, C.A., 2021. Understanding aqueous and non-aqueous proton T1 relaxation in brain. J. Magn. Reson. 323, 106909.

Ma, Y., et al., 2018. Accurate T1 mapping of short T2 tissues using a three-dimensional ultrashort echo time cones actual flip angle imaging-variable repetition time (3D UTE-Cones AFI-VTR) method. Magn. Reson. Med. 80, 598–608.

Reynolds, L.A., et al., 2023. Non-aqueous magnetization following adiabatic and selective pulses in brain: T1 and cross-relaxation dynamics. NMR Biomed e4936.

Luk, B.T., Zhang, L., 2015. Cell membrane-camouflaged nanoparticles for drug delivery. J. Control. Release 220, 600–607.

Xia, Q., Zhang, Y., Li, Z., Hou, X., Feng, N, 2019. Red blood cell membrane-camouflaged nanoparticles: a novel drug delivery system for antitumor application. Acta Pharm. Sin. B 9, 675–689.